Archives of Materials Science and Engineering

Volume 67
Issue 2
June 2014
Pages 60-69

International Scientific Journal
published monthly by the
World Academy of Materials
and Manufacturing Engineering

The effect of silicon content on the pitting corrosion of duplex stainless steel weldment

B.H. Lee, H.J. Lee, D.W. Kang, H.W. Lee*
Department of Materials Science and Engineering, Dong-A University,
840 Hadan-dong, Saha-gu, Busan 604-714, Republic of Korea
* Corresponding e-mail address: hwlee@dau.ac.kr

Received 26.03.2014; published in revised form 01.06.2014

ABSTRACT

Purpose: In this study, the effect of Si content at a welded DSS on the pitting resistance was investigated.

Design/methodology/approach: The δ-ferrite fraction increased due to addition of Si, and the amount of γ_2 decreased. In the ferric chloride pitting test, the weight reduction range decreased due to an increase in the Si content. As to the location, pittings occurred intensively at the grain boundary or within the austenite grain due to the difference in PREN caused by the differential solid solubility in each phase.

Findings: As a result of the potentiodynamic polarization test, while the E_{pit} (Critical Pitting Potential) of all specimens depending on the temperature were observed to be similar at room temperature up to 45°C, the reduction range of the Epit was found to be small at the temperature higher than 45°C as Si content increased. This was found to be because of formation of SiO_2 in the passive film.

Research limitations/implications: Higher the addition of Si, the more the number of pittings generated at the grain boundary decreased as the coherence of the passive film increased by the Si accumulated at the boundary.

Originality/value: In this study, we intend to investigate the effect of Si element addition on the pitting resistance of the duplex stainless steel welding zone.

Keywords: Duplex stainless steel; Pitting corrosion; Silicon; Potentiodynamic polarization tests

Reference to this paper should be given in the following way:

B.H. Lee, H.J. Lee, D.W. Kang, H.W. Lee, The effect of silicon content on the pitting corrosion of duplex stainless steel weldment, Archives of Materials Science and Engineering 67/2 (2014) 60-69.

PROPERTIES

1. Introduction

Duplex stainless steel has a microstructure in which δ-ferrite and austenite (γ) phases are mixed almost equally at a one to one ratio, and it has excellent mechanical properties, machinability and corrosion resistance. Thus, it is widely used for chemical apparatuses, offshore platform and pipelines for marine plants. It is also applied to desalination facilities, chemical material carriers and

desulfurization facilities in Korea, and, as its application is expected to be expanded, highly strong materials with superior corrosion resistance like duplex stainless steel are receiving attention like the industrial materials that can accustom to extreme environments. In particular, duplex stainless steel has very superior resistance characteristics against pitting corrosion, crevice corrosion, and chlorine-caused stress corrosion cracking to austenitic stainless steel such as 304 and 316 [1-3].

Due to the trend of replacing austenitic stainless steel such as 304 and 316 with duplex stainless steel which requires relatively small addition of Ni caused by the increase in the price of nickel in 2006, the application scope of duplex stainless steel is expanding recently increasing the demand for duplex stainless steel by 20% or more every year [4,5].

PREN (Pitting Resistance Equivalent Number) which is one of the biggest advantages of duplex stainless steel is widely used as the value to evaluate the resistance to pitting in an overall corrosive environment, and the equation is as shown in (1) below:

$$PREN = wt.\%Cr + 3.3wt.\%Mo + 30wt.\%N \quad (1)$$

As seen in Equation (1), Cr, Mo and N act as important factors which improve pitting resistance, and, besides, W, Si, V and Ni are known to be the elements which improve pitting resistance [6]. Also, the CPT (Critical Pitting Temperature) obtained through an electrochemical test [7] or a chemical test [8] is also used as a criterion to evaluate pitting resistance, among which ASTM G48 [8] is used as the criterion for CPT measurement through a chemical test in a 10%$FeCl_3$ solution. A high CPT value of duplex stainless steel means superior pitting resistance, and, the higher the E_{pit} (Critical Pitting Potential) is in a potentiodynamic polarization test at the determined CPT, the more superior the pitting resistance is evaluated to be [9].

At present, while studies on the effect of Mo, N, W, etc. on pitting resistance are actively conducted through the studies conducted on quality and welding technology as the application scope of duplex stainless steel is expanded [10-12], there are insufficient studies on Si. Accordingly, in this study, we intend to investigate the effect of Si element addition on the pitting resistance of the duplex stainless steel welding zone.

2. Experimental procedure

2.1. Welding consumable and welding

The welding was conducted by the FCAW (Flux Cored Arc Welding) method using a specimen of size 500 mm x 240 mm x 20 mm made of base material, stainless steel 304. The welding wires were produced fixing the contents of Cr, Mo, Ni, Mn and N and changing the content of Si to 0.6wt.%, 0.9wt.% and 1.8wt.%. After conducting buttering welding once in order to minimize the effect of the base material, a 12 pass welding was conducted as shown in Fig. 1 attaching a backing strip in the conditions of the root gap of 12 mm, groove angle of 45°, CO_2 100% as the shielding gas, and flow rate of 20 L/min. As to the current, DCRP (Direct Current Reverse Polarity) was used. The welding condition of each specimen is shown in Table 1.

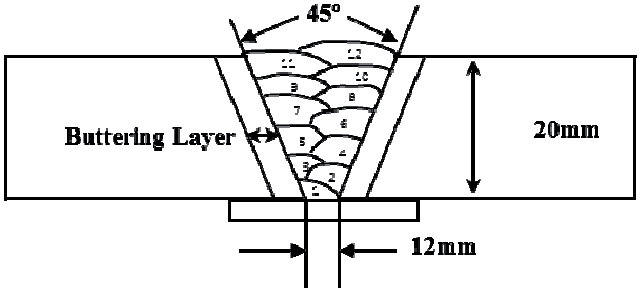

Fig. 1. Schematic diagram of the weldment

Table 1.
Welding parameters

	Voltage, V	Current, A	Travel speed, cm/min	Heat input, kJ/cm	Interpass temperature, °C	pass
No.1	30	200	35	10.4	Max. 150	12
No.2	30	200	35	10.4	Max. 150	12
No.3	30	200	34	11.0	Max. 150	12

In order to observe the microstructure using an optical microscope and SEM (Scanning Electron Microscope), specimens were taken from the deposited metal, which was electrolytically etched for 15 seconds at 3 V using 10% oxalic acid after grinding and polishing.

2.2. Phase component analysis

An optical emission spectrometer (Metal-Lab75/80J, GNR srl, Italy) and the nitrogen analyser (ELTRA Oxygen/Nitrogen Determinator ON-900, ELTRA GmbH. Co.) were used to measure the chemical composition of the specimens, and the mean values were calculated after making the measurement 10 times per specimen in order to reduce the error range. The result is shown in Table 2.

Table 2.
Chemical composition of the weld metal (wt%)

	C	N	Si	Mn	P	S	Cr	Ni	Mo	FN	PREN
No. 1	0.03	0.14	0.65	1.02	0.025	0.003	22.09	9.49	3.48	33	36.7
No. 2	0.03	0.14	0.89	1.02	0.025	0.004	22.42	9.5	3.31	39	36.6
No. 3	0.05	0.14	1.76	0.98	0.025	0.004	23.16	9.15	3.07	53	36.6

Also, the δ phase and γ phase ingredients in the deposited metal were analyzed 10 times respectively using an EDS (Energy Dispersive X-ray Spectrometer) and the mean values were calculated, and the equipment used was a Scanning Electron Microscopy with an Energy Dispersive Spectroscopy (SEM-EDS) (JSM-6700f, jeol, Japan) at the acceleration voltage was 20 kV and the spot size was set to 3.0.

2.3. Ferric chloride pitting test

A ferric chloride pitting test was conducted in accordance with ASTM G48-11 Method E [8]. The equation used to determine the CPT is as shown in (2):

$$CPT\ °C = (2.5 \times wt.\%Cr) + (7.6 \times wt.\ \%Mo) + + (31.9 \times wt.\%N) - 41.0 \quad (2)$$

The test was conducted by taking specimens of size 2.54 cm x 2.54 cm from the deposited metal, which was ground, polished and weighed before conducting the test. The tests were conducted at 45°C (±1°C) for 24 hours after charging '600 ml of 6 % $FeCl_3$ + 1 % HCl solution' and a specimen into each container. After completion of the tests, the rust on the specimen surfaces was cleaned using distilled water and then by an ultrasonic cleaner using ethanol. The tested specimens were measured to calculate the loss by comparing the values before and after the test, and electrochemical etching in oxalic acid for the formed pitting observations on the surfaces through SEM.

2.4. Pitting corrosion resistance test

In order to test the electrochemical characteristics of the specimens, potentiodynamic polarization tests were conducted using an electrochemical analyzer (VersaSTAT 3 Potentiostat Galvanostat, Princeton Applied Research). Prior to each experiment, all specimens was ground by 2000-grit SiC polishing paper, cleaned ultrasonic cleaner using ethanol. Rinsed with distilled water, and dried in air. Before the potentiodynamic polarization test, each specimens were immersed in the electrolytes for at least 20 min for stabilization of the OCP (Open Circuit Potential). The tests were conducted at temperatures of 25, 35, 45, 55 and 65°C respectively, and 3.5% NaCl was used as the electrolyte, the range of the potential was set to -0.7 to 1.5 V, and the scanning speed to 0.4 V/s. The working electrode of the potentiodynamic polarization test was each specimen, an Ag-AgCl/KCl-sat's (0.197 Volts) electrode was used as the reference electrode, and a platinum foil was used as the counter electrode.

3. Result and discussion

3.1. Microstructure

Figure 2 shows the microstructure which differ depending on the Si contents of the duplex stainless steel weld metals. The microstructure of duplex stainless steel was observed to be in the form where γ is floating like an island on the matrix of δ-ferrite. As the content of Si increased from 0.6wt.% to 0.9wt.% and 1.8% respectively, the value of Cr_{eq}/Ni_{eq} increased from 1.76 to 1.79 and 1.88, and the δ-ferrite content of the weld zone also increased from 31% to 36% and 47%. According to a preceding study, the fractions of δ-ferrite and γ increase or decrease depending on each element added, and the alloy elements which have an effect on formation of the phase are as follows [13]:

- Austenite formers: Ni, C, N, Mn, Co and Cu,
- Ferrite formers: Cr, Mo, Si, Nb, Ti, Al, W, V and Ta.

Like this, Si increases the δ phase fraction of duplex stainless steel when it is added as a ferrite former, which is achieved by the increase in Cr_{eq}/Ni_{eq}, and the equation is shown in (3):

$$Cr_{eq} = \%Cr + \%Mo + (1.5 \times \%Si) + (0.5 \times \%Nb)$$
$$Ni_{eq} = \%Ni + (0.5 \times \%Mn) + (3 \times \%C) + (30 \times \%N) \quad (3)$$

Due to the increase in the value of Cr_{eq}/Ni_{eq} calculated in Equation (3), the composition of the duplex stainless steel in the pseudo-binary phase diagram of Fig. 3 is moved to the right, as a result of which the δ-ferrite solvus line descends. Accordingly, the duration in the section where γ is formed after welding becomes shorter, due to which the fraction of δ-ferrite increases.

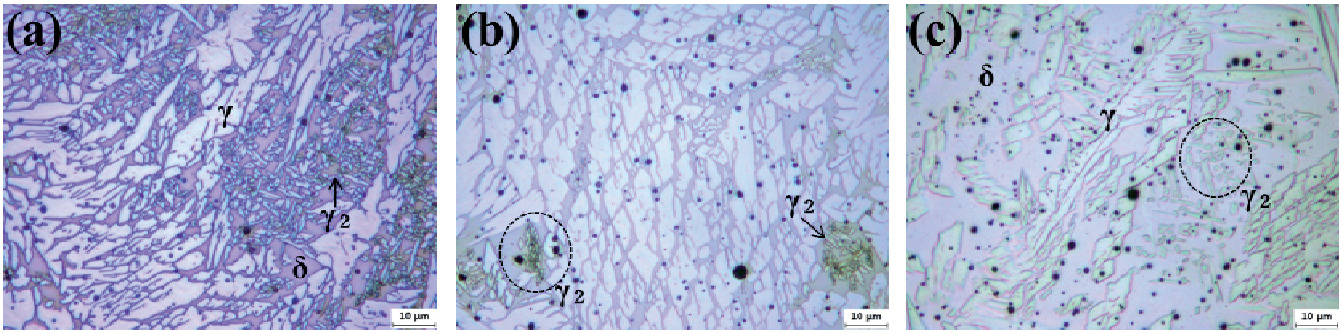

Fig. 2. Microstructure of weldments : a) No. 1, b) No. 2, c) No. 3

The microstructures of specimens No. 1, 2 and 3 are shown to have grown along the grain boundary of δ-ferrite in the form of Widmanstätten Austenite, and the amount of γ_2 has decreased as the Si content has increased. In a preceding study, γ_2 was a location where pitting occurs because the N content of γ_2 is 1/2 compared with the existing γ [14]. Also, the more the Si content increased, thin Widmanstätten Austenite was formed, and γ grew with a certain directionality in Specimen No. 1 and No. 2. Such directionality relation between the metamorphoses of δ-ferrite and γ has been verified through Kudjumov-Sachs relationship ($<111>_\alpha // <110>_\gamma$ and $\{110\}_\alpha // \{111\}_\gamma$) [15].

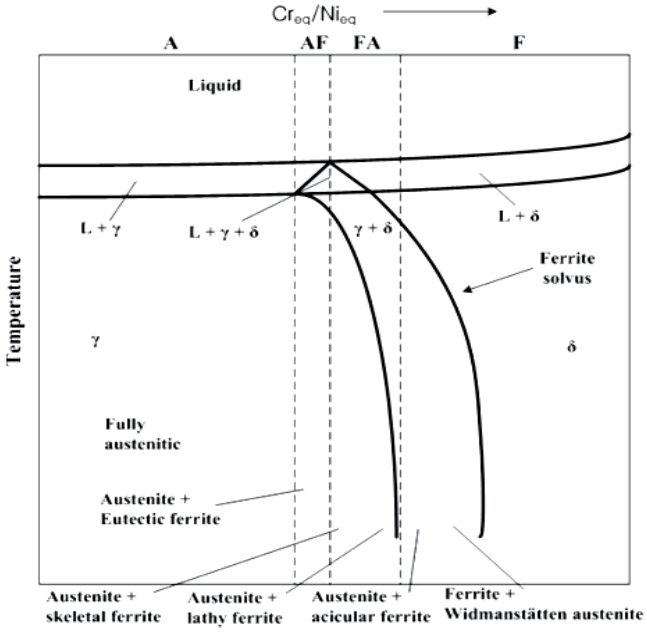

Fig. 3. Pseudo-binary Fe-Cr-Ni phase diagram

3.2. Pitting resistance properties

In order to observe the effect of reduction in the amount of γ_2 on pitting, a Ferric Chloride Pitting test was conducted for 24 hours at 45°C in 6% $FeCl_3$ + 1% HCl solution. The change in the weight of each specimen after the ferric chloride pitting test which differs depending on the Si content was shown in Table 3. The mass loss of specimen No. 1 of which the Si addition was 0.6wt.% was 6.1%, and the weight was observed to have decreased by 5.4% and 4.7% respectively as the Si content increased to 0.9wt.% and 1.8wt.%. Fig. 4. Shows SEM images of the each specimens after the ferric chloride pitting test for observing the shape of pittings.

Table 3.
Mass loss of each specimens in CPT test

	Before CPT, g	After CPT, g	Mass loss, %
No. 1	28.788	27.031	6.067
No. 2	24.833	23.480	5.446
No. 3	29.825	27.908	4.701

Pittings occurred in specimens a, b and c in Fig. 4, and the pitting forms were observed to be undercutting, subsurface, etc. in accordance with ASTM G46. [16] Also, much δ-ferrite is observed around the pittings, through which it is presumed that growth of pitting is delayed or stopped when it approaches δ-ferrite. Figure 5 shows the result of observing the surface through a SEM after conducting a potentiodynamic polarization test up to 1.250 V in order to find the location where the first pitting has occurred.

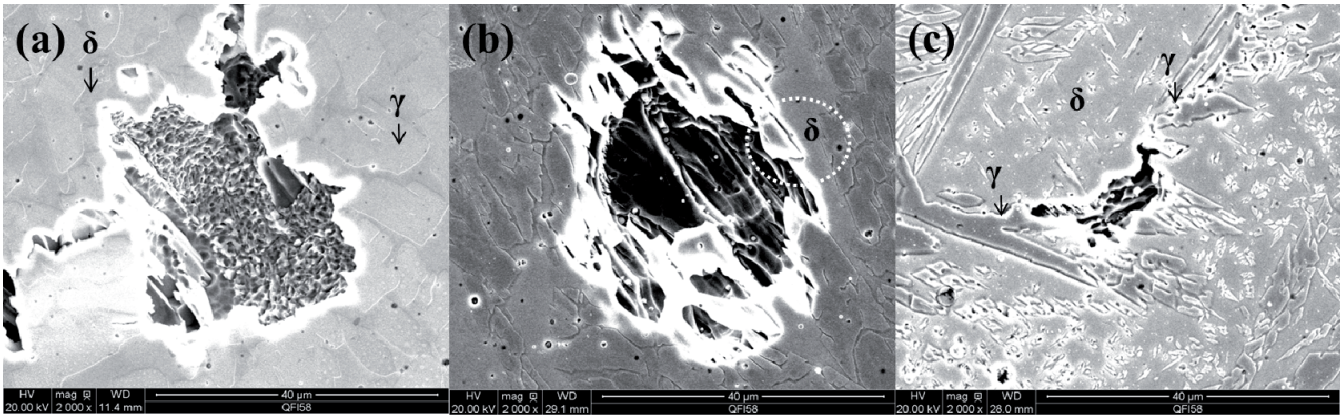

Fig. 4. SEM morphologies of pits formed each specimens after CPT test in 6% $FeCl_3$ + 1% HCl solution: a) No. 1, b) No. 2, c) No. 3

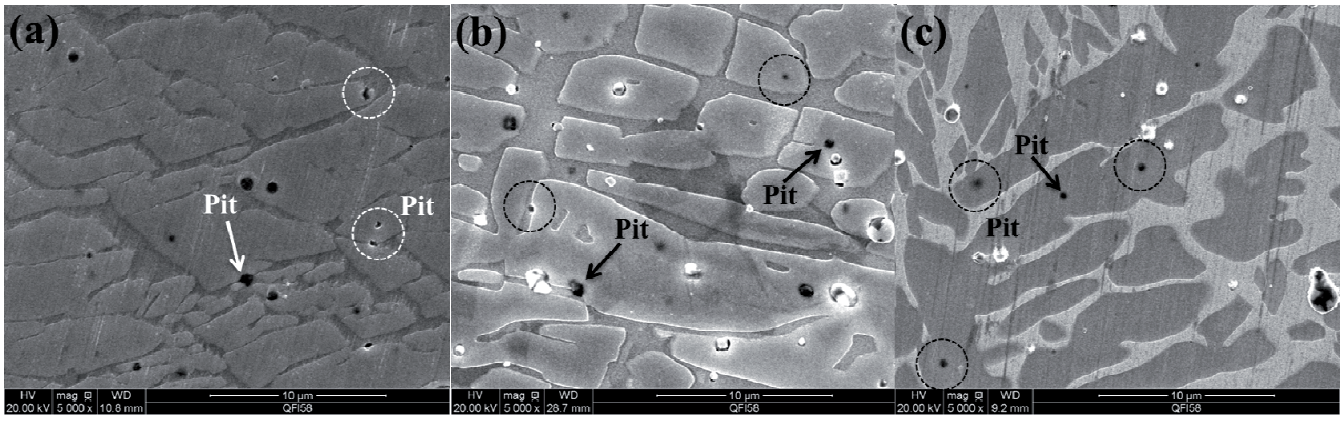

Fig. 5. SEM morphologies of pits formed each specimens during the potentiodynamic test at 1250 mV in 3.5% NaCl: a) No. 1, b) No. 2, c) No. 3

The result of the test showed that pittings occurred selectively at the boundary of δ-ferrite//γ, inside of γ, or at γ_2. That is to say, pittings occur inside γ, boundary of δ-ferrite//γ and at γ_2, and their growth is delayed when it meets the δ-ferrite phase. Fig. 6 shows the result of observing inside pitting through SEM & EDS. As a result of EDS measurement, δ-ferrite phase is observed inside a pitting, which supports to the earlier finding that a pitting stops growing when it contacts with the δ-ferrite phase. Also, a preceding study explains that pittings selectively occur at γ as a result of the difference in PREN between δ-ferrite and γ caused by the differential solid solubility of alloy elements in each phases [17]. And according to Bae [18], occurrence of pitting at the grain boundary is due to decrease in the PREN value at the grain boundary resulting from the local decline in the Cr content. In order to determine this difference, a phase component analysis was performed with EDS and which result is shown in Table 4. Also the PREN value in each phase was corrected through Equation (1).

The contents of the alloy elements of δ-ferrite and γ were differently observed in all the specimens, among which Cr and Mo in each phase were much different from each other by 1-3wt.% and 0.9-1.9wt.% respectively, and thus PREN also showed a big difference of 2 to 4. As for the Si content in δ-ferrite was observed to be much higher than in γ same as the Cr and Mo contents, but it is presumed that Si content had no big effect on the pittings were occurred because Si is not directly involved in PREN. However, in specimen No. 3 which has the highest Si content, the frequency of pitting occurrence at the grain boundary was decreased. This is presumed to be because of Si, and there is the result of measuring Si contents of each phase by line

scanning as shown in Fig. 7. The Si content is higher in the δ-ferrite of a dark color than in γ of a bright color, and it can be seen that the Si content is higher at the grain boundary in particular. This is due to the low diffusion speed of Si. In a preceding study, Si added in stainless steel is known to strengthen the passive film by forming SiO_2 [19]. Though pittings occur at the grain boundary due to a low PREN value resulting from the Cr content, the number of pittings which occur at the grain boundary decreases because the passive film is reinforced by the Si accumulated at the grain boundary as the Si content increases.

Table 4.
Chemical composition of Ferrite and Austenite phases in each specimens

	Phase	Cr	Mo	N	Si	PREN
No. 1	Austenite	22.06	3.22	0.14	0.75	35.92
	Ferrite	23.32	4.10	0.06	1.07	37.42
No. 2	Austenite	22.44	3.40	0.14	0.84	36.84
	Ferrite	25.10	4.73	0.05	1.13	40.79
No. 3	Austenite	22.57	3.10	0.14	1.74	36.07
	Ferrite	24.76	4.20	0.05	1.93	38.86

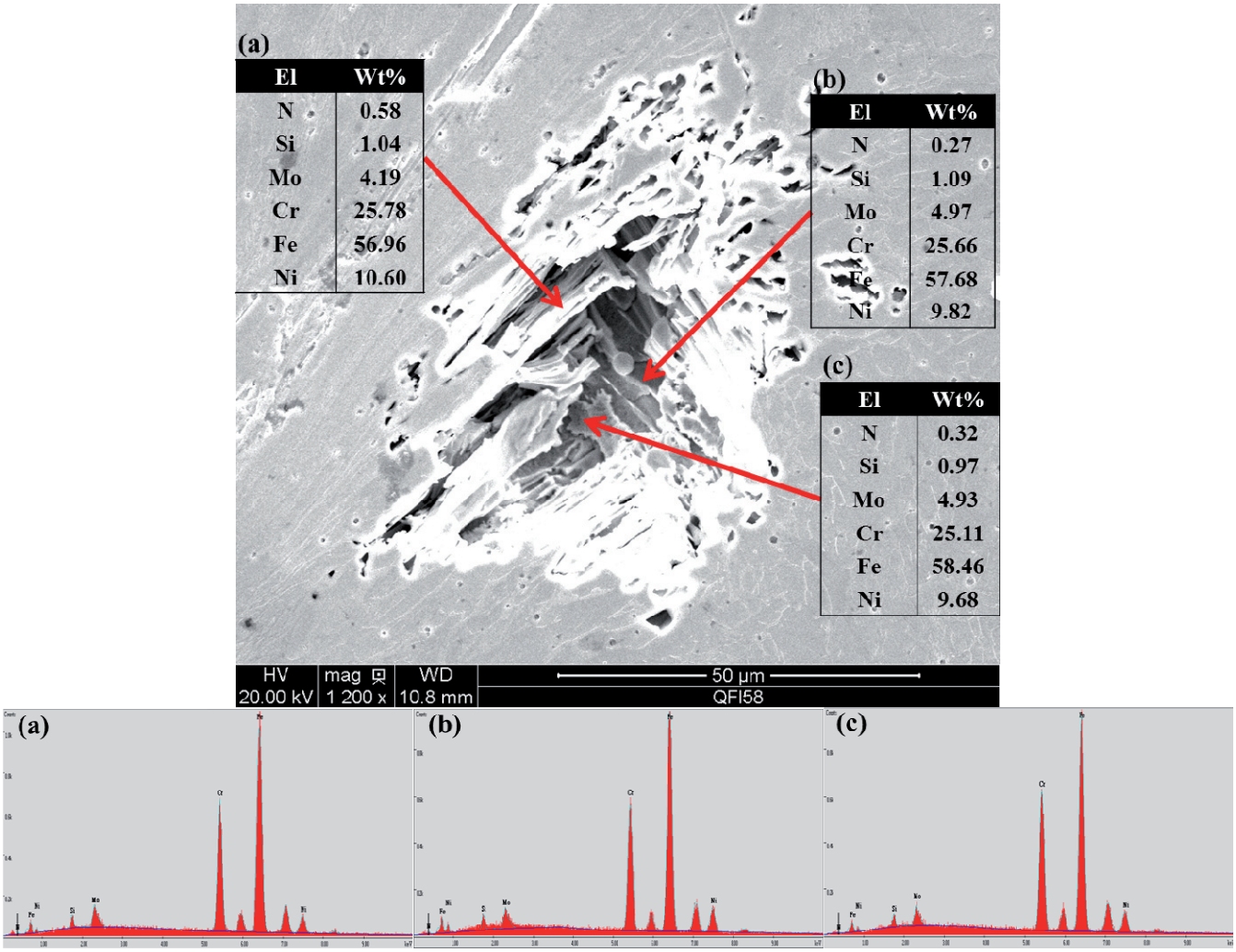

Fig. 6. SEM & EDS measurements of δ-ferrite formed inside the pit

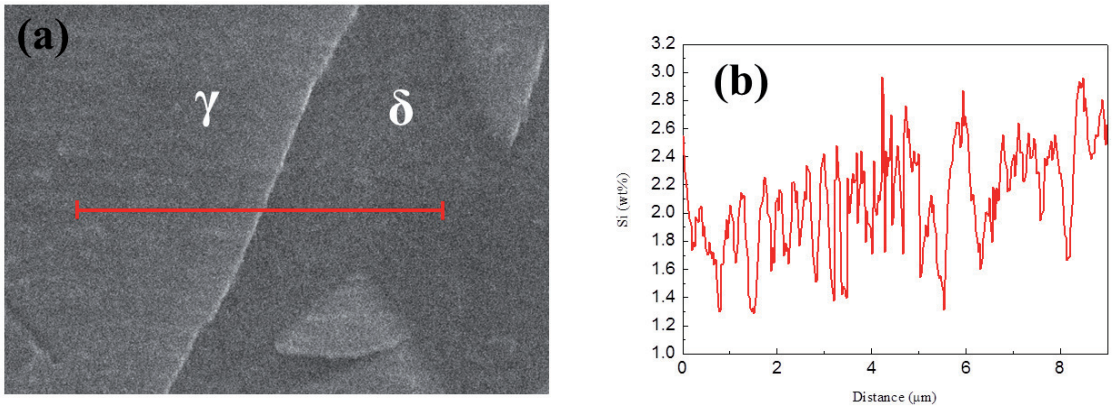

Fig. 7. Mapping analysis of γ//δ-ferrite grain boundary

In order to observe the increase in the pitting resistance resulting from increase in the Si content, potentiodynamic polarization tests were conducted for each specimen in 3.5%NaCl at 25, 35, 45, 55, and 65°C; the result is shown in Fig. 8 and electrochemical parameters were listed in Table 5.

Overall, the resulting polarization curve was typical of DSS. The E_{pit} of all the specimens were observed to be the same at 25°C as 1190 mV. However, the E_{pit} values were observed to be different at 35, 45, 55 and 65°C in each specimens. First, No. 1 which has the smallest the Si contents, while a minor change in the E_{pit} was observed as the temperature increased up to 35°C. On the other hand, the range of decline in the E_{pit} was observed to have been big as the temperature increased above 45°C. In the case of No. 2 specimen with 0.9wt.% Si, the polarization curve was also formed as the same appearance with specimen No. 1. But, No. 3 specimen which has the biggest Si content, was observed minor change in the E_{pit} as the temperature increased until 45°C. And above 55°C, a little decrease of E_{pit} was observed.

In the Table 5, the value of E_{corr}, I_{corr}, b_c, b_a, K_{corr} were determined from polarization measurement through Versa Studio software. For calculating these parameters, the value of the equivalent weight of each specimens (Ew: No. 1 – 3558.619, No. 2 – 3548.24 No. 3 – 3530.709 grams/equivalent), the density (D: No. 1 – 7.65, No. 2 – 7.61, No. 3 – 7.44 g/cm^2) had to be inserted to the software. The values of cathodic, I_{corr} and anodic currents and K_{corr} (corrosion rate) are decreased with increasing Si contents in each temperature. Also, both b_c and b_a as well as shifted E_{pit} values are moved positive values. This was because the decreasing the general dissolution and pitting corrosion of the alloy through decreasing the rate of the anodic and cathodic reaction [20].

The cathodic reaction of alloy in aerated NaCl solutions is the oxygen reaction [21]. And it is generally believed that the anodic reaction of alloy in same condition is the dissolution of iron. When metal corrodes, both reactions take place at the same time. The reaction formulas are shown in (4):

$$\text{Anodic : } Fe \rightarrow Fe^{2+} + 2e^-$$
$$\text{Cathodic : } 2H_2O + O_2 + 4e^- \rightarrow 4OH^- \quad (4)$$

These both reactions are reduced by the silicon addition and the positive values of electrochemical parameters are mainly due to the formation of thin and compact oxide film. In the preceding study, the surface film was observed by XPS, which was consisted chromium oxide (Cr_2O_3), silicon oxide (SiO_2), iron oxide (Fe_2O_3) in DSS [22]. It is well known that the chromium improves resistance of Fe-base alloy to general and pitting corrosion by formation of the passive film [23,24]. Also, Si-rich film on the surface efficiently prevent the pitting corrosion [25]. The effect of silicon addition was easy to know through the changing of E_{pit} value in each temperature.

Figure 9 shows the relationship between the E_{pit}, the criterion for pitting resistance, and temperature for each specimens. The CPT is that at which the pitting potential drops. In this test, the value of 900mV was fixed as the lower limit. From this rule, the CPT values of each specimens are placed in the 35 to 45°C range. That is similar with the CPT calculated by Equation (2) from the ASTM G-48 [8]. In No. 3 specimen, the E_{pit} approached the minimum value above 45°C. And also the E_{pit} values at 55°C and 65°C were observed to be much higher than other specimens. It has been reported by studies that, in general, Cr, Mo, N and Si are closely related to the value of E_{pit} [6]. Among those, Si increases E_{pit} by existing in a passive film

as forming a SiO_2 film between the passive film and the metal surface [26]. Also, the amount of the oxidation layer on a corroded metal surface is known to increase as the amount of Si increases [27]. Table 6 shows the Si contents on the tested specimen surfaces through EDS for proof previous studies. The result of EDS analysis showed that the Si content on the specimen surfaces much increased after the potentiodynamic polarization test at each temperature. This was because Si participated in formation of the passive film, due to which the pitting resistance was improved.

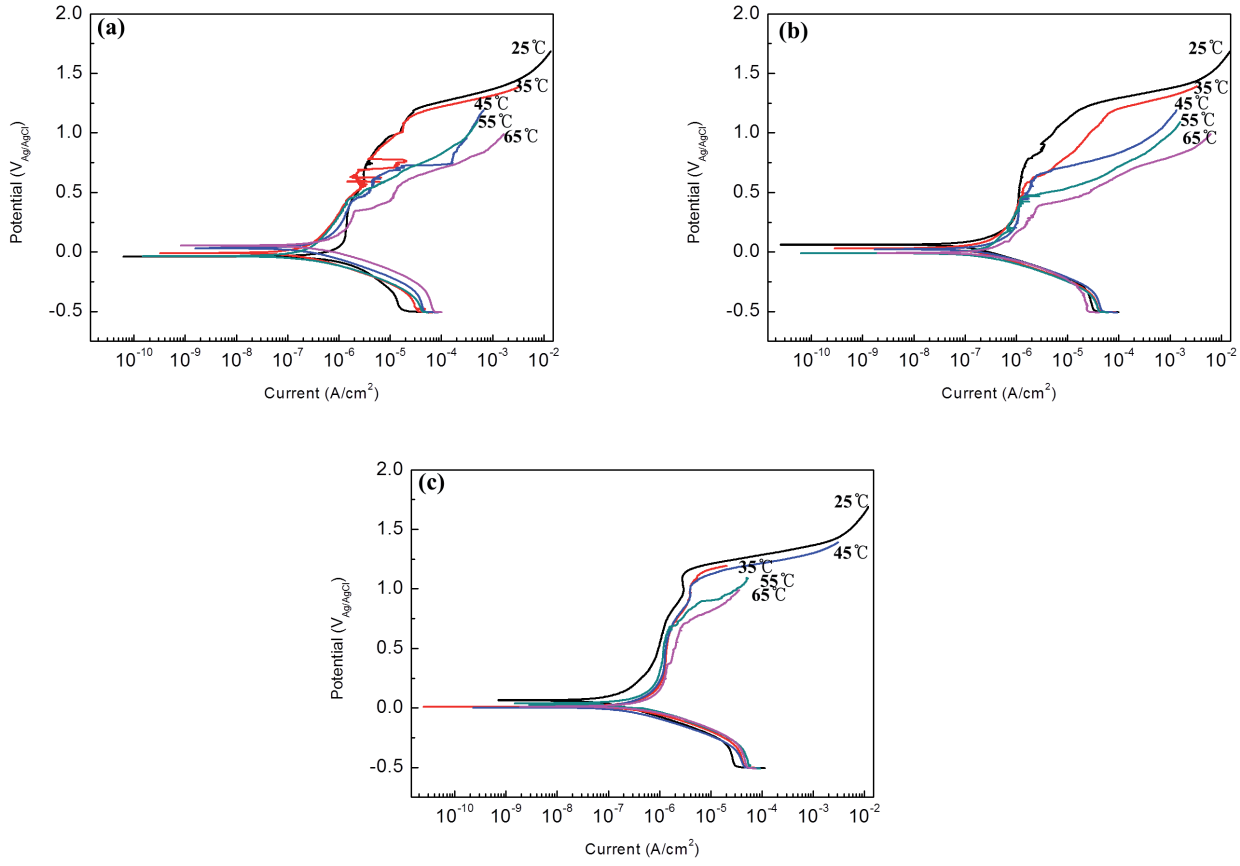

Fig. 8. Polarization curve of each specimens in 25°C, 35°C, 45°C, 55°C , 65°C , 3.5% NaCl: a) No. 1, b) No. 2, c) No. 3

Table 5.
Corrosion parameters of the DSS weldments tested in 0.5M NaCl solution

		E_{corr}, mV	I_{corr}, μA/cm^2	b_c, mV/dec	b_a, mV/dec	E_{pit}, mV	Corrosion rate, mpy
25°C	No. 1	55.662	308.175	159.33	494.267	1188.888	18.096
	No. 2	56.462	294.921	162.519	495.954	1195.942	17.708
	No. 3	60.308	172.824	188.723	556.398	1194.716	10.555
45°C	No. 1	13.118	552.256	136.503	4293510	630.069	33.099
	No. 2	20.647	534.821	141.470	436.759	646.018	32.112
	No. 3	43.409	372.576	151.450	476.319	1048.417	22.775
65°C	No. 1	-16.341	633.483	117.878	374.247	440.525	37.967
	No. 2	-8.464	608.141	118.921	392.561	457.393	36.549
	No. 3	25.378	508.157	151.660	453.170	680.369	31.063

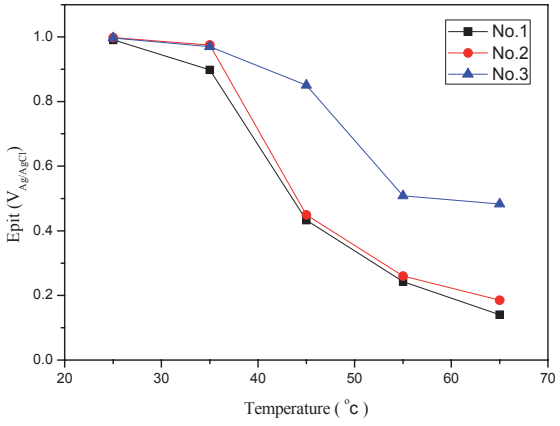

Fig. 9. Pitting potential (E_{pit}) against temperature in each specimens

Table 5.
The change of silicon composition each specimen after potentio dynamic polarization at different temperature

Si, wt%	No. 1	No. 2	No. 3
As-weld	0.6	0.9	1.8
25°C	0.72	0.93	1.9
45°C	0.75	0.13	1.9
65°C	0.87	1.15	1.9

4. Conclusions

1) The result of observing the microstructure showed that, the more the Si content increased, the more the value of Cr_{eq}/Ni_{eq} increased, due to which the fraction of δ-ferrite increased and the amount of γ_2 decreased. In the specimens, No. 1, No. 2, γ was formed along the grain boundary of δ-ferrite with certain directionality.
2) In the ferric chloride pitting test at 45°C, mass loss was reduced as the Si addition increased.
3) The location where pittings occur is determined by the PREN value between the two phases which results from the Cr, Mo, and N differentially contained as solid in δ-ferrite and γ. Accordingly, pittings occur inside the grain of γ or at the grain boundary where the PREN value is low, and go along encroaching γ until δ-ferrite is approached. Though Si is not directly involved in the location where pittings occur, it reduces occurrence of pittings at the grain boundary as it is accumulated at the grain boundary to form SiO_2.
4) As a result of potentiodynamic polarization tests conducted at high temperatures, while the same E_{pit} was observed with all the three specimens in 3.5%NaCl at 25°C, the decrease range changed as the temperature increased. While the E_{pit} of specimens No. 1 and 2 were maintained at somewhat decreased values as the temperature increased up to 35°C, they showed a rapid decrease between 35 and 45°C. The decrease in the E_{pit} of specimen No. 3 was small up to 35°C, and the value was observed to be higher than those of specimens No. 1 and 2 also at the temperature of 45°C or higher.
5) The increase in the Si content on the specimen surfaces after the potentiodynamic polarization tests was due to formation of SiO_2 in the passive film, as a result of which the Si content increased making the E_{pit} increase at high temperature.

Acknowledgements

The present research was financially supported by the Ministry of Education, Science Technology (MEST) and National Research Foundation of Korea (NRF) through the Human Resource Training Project for Regional Innovation.

References

[1] J.O. Nilsson, Super duplex stainless steels, Materials Science and Technology 8/ (1992) 685-700.
[2] S.-K. Ahn, J.-S. Kim, K.-T. Kim, Journal of KWS 22 (2010) 22.
[3] B. Deng, Y. Jiang, J. Gong, Ch. Zhong, J. Gao, J. Li, Critical pitting and repassivation temperatures for duplex stainless steel in chloride solutions, Electrochimica Acta 53/16 (2008) 5220-5225.
[4] J. Chater, The Irresistible Rise of Duplex, Stainless Steel World December (2007) 48-51.
[5] F. Eghbali, M.H. Moayed, A. Davoodi, N. Ebrahimi, Critical pitting temperature (CPT) assessment of 2205 duplex stainless steel in 0.1 M NaCl at various molybdate concentrations, Corrosion Science 53/1 (2011) 513-522.
[6] R.N Gunn, Duplex Stainless Steel, Woodhead Publishing Ltd, Abinton, 1997.
[7] V.M. Linton, N.J. Laycock, S.J. Thomsen, A. Klumpers, Failure of a super duplex stainless steel reaction vessel, Engineering Failure Analysis 11/2 (2004) 243-256.
[8] ASTM Standard G48-11, Standard Test Methods for Pitting and Crevice Corrosion Resistance of Stainless Steels and Related Alloys by use of Ferric Chloride Solution, ASTM, Philadelphia, 2011.

[9] A.J. Sedriks, Corrosion of stainless steels, Wiley & Sons, Inc., New York, 1996.
[10] N.D. Tomashov, G.P. Chernova, O.N. Marcova, Effect of Supplementary Alloying Elements On Pitting Corrosion Susceptibility Of 18Cr-14Ni Stainless Steel, Corrosion 20/5 (1964) 166t-173t.
[11] R. Merello, F.J. Botana, J. Botella, M.V. Matres, M. Marcos, Influence of chemical composition on the pitting corrosion resistance of non-standard low-Ni high-Mn-N duplex stainless steels, Corrosion Science 45/5 (2003) 909-921.
[12] J.H. Potgiter, P.A. Olubambi, L. Cornish, C.N. Machio, E.M. Sherif, Influence of nickel additions on the corrosion behaviour of low nitrogen 22% Cr series duplex stainless steels, Corrosion Science 50/9 (2008) 2572-2579.
[13] I. Alvarez-Armas, S. Degallaix-Moreuil, Duplex Stainless Steel, ISTE Ltd and Wiley & Sons, Inc., London and Hoboken, 2009.
[14] J.C. Lippold, D.J. Kotecki, Welding Metallurgy and Weldability of Stainless Steels, Wiley & Sons, Inc., Hoboken, 2005.
[15] D.N. Lee, H.N. Han, Directed growth of ferrite in austenite and Kurdjumov-Sachs orientation relationship, Materials Science Forum 715-716 (2012) 128-133.
[16] ASTM Standard G 46-94, Standard Guide for Examination and Evaluation of Pitting Corrosion, ASTM, Philadelphia, 2005.
[17] Y. Jang, S. Kim, J. Lee, Effect of different mo contents on tensile and corrosion behaviors of CD4MCU cast duplex stainless steels, Metallurgical and Materials Transactions A 36/5 (2005) 1229-1236.
[18] S.H. Bae, H.W. Lee, Effect of Mo contents on corrosion behaviors of welded duplex stainless steel, Metals and Materials International 19/3 (2013) 563-569.
[19] J.S. Dunning, D.E. Alman, Oxidation and Sulfidation Resistant Alloys with Silicon Additions, NETL, Pittsburgh, 2003.
[20] P. Baradlai, J.H. Potgieter, W.O. Barnard, L. Tomcsanyi, K. Varga, Investigation of Spontaneous Passivation of Stainless Steels Modified with Ruthenium, Materials Science Forum 185-188 (1995) 759-768.
[21] E.M. Sherif, Effects of 2-amino-5-(ethylthio)-1,3,4-thiadiazole on copper corrosion as a corrosion inhibitor in 3% NaCl solutions, Applied Surface Science 252/24 (2006) 8615-8623.
[22] J.E. May, C.A.C. de Sousa, S.E. Kuri, Aspects of the anodic behaviour of duplex stainless steels aged for long periods at low temperatures, Corrosion Science 45/7 (2003) 1395-1403.
[23] M. Bojinov, G. Fabricius, T. Laitinen, T. Saario, G. Sundholm, Conduction mechanism of the anodic film on chromium in acidic sulphate solutions, Electrochimica Acta 44/2-3 (1998) 247-261.
[24] H. Tsuchiya, S. Fujimoto, O. Chihara, T. Shibata, Semiconductive behavior of passive films formed on pure Cr and Fe-Cr alloys in sulfuric acid solution, Electrochimica Acta 47/27 (2002) 4357-4366.
[25] A.A. Hermas, K. Ogura, S. Takagi, T. Adachi, Effects of Alloying Additions on Corrosion and Passivation Behaviors of Type 304 Stainless Steel, Corrosion 51/1 (1995) 3-10.
[26] J.S. Armijo, B.E. Wilde, Influence of Si content on the corrosion resistance of austenitic Fe-Cr-Ni alloys in oxidizing acids, Corrosion Science 8/9 (1968) 649-664.
[27] B.E. Wilde, Influence of Silicon on the Intergranular Corrosion Behavior of 18Cr-8Ni Stainless Steels, Corrosion 44/10 (1988) 699-704.